

Enabling Variable High Spatial Resolution Retrieval From a Long Pulse BOTDA Sensor

Zhao Ge, Li Shen, Can Zhao^{ID}, Hao Wu^{ID}, Zhiyong Zhao^{ID}, Member, IEEE,
and Ming Tang^{ID}, Senior Member, IEEE

Abstract—Spatial resolution (SR) is one of the most important parameters of Brillouin optical time-domain analysis (BOTDA) sensors, which determines the minimum length that a perturbation event can be distinguished. In the field of Internet of Things (IoT), there is an urgent need for sensors with large-scale high-precision sensing capability for scenarios, such as intelligent monitoring of production lines and urban infrastructure. Conventionally, the SR is normally restricted to be longer than 1 m due to the ~10-ns acoustic lifetime limitation in silica optical fibers. For long-distance smart monitoring systems, the SR is generally on the order of several meters or even worse. However, it does not meet the needs of many applications. Therefore, there is an urgent need to achieve SR in the submeter magnitude. In this work, for the first time to the best of our knowledge, we propose a convolutional neural network (CNN) to process the data of conventional BOTDA sensors, which achieves unprecedented performance improvement that allows to directly retrieve submeter SR from the sensing system that use long pump pulses. By using the simulated Brillouin gain spectrums (BGSs) as the CNN input and the corresponding high SR Brillouin frequency shift (BFS) as the output target, the trained CNN is able to obtain an SR higher than the theoretical value determined by the pump pulse width. In the experiment, the CNN accurately retrieves 0.5-m hotspots from the measured BGS with pump pulses from 20 to 50 ns, and the acquired BFS is in great agreement with 45/40 ns differential pulse-width pair (DPP) measurement results. Compared with the DPP technique, the proposed CNN demonstrates a twofold improvement in BFS uncertainty with only half the measurement time. In addition, by changing the training data sets, the proposed CNN can obtain tunable high SR retrieval based on conventional BOTDA sensors that use long pulses without any requirement of hardware modifications. It is worth mentioning that the proposed method is also applicable to larger pulse widths to retrieve a submeter SR. The proposed data post-processing approach paves the way to enable novel high SR BOTDA sensors, which brings substantial improvement

over the state-of-the-art techniques in terms of system complexity, measurement time, reliability, etc.

Index Terms—Brillouin scattering, convolutional neural network (CNN), distributed optical fiber sensors, signal processing.

I. INTRODUCTION

WITH the development of smart factories, smart cities, industrial Internet of Things (IoT), etc., the IoT has dramatically changed our lives. Brillouin optical time-domain analysis (BOTDA) can measure the temperature and strain distribution along the optical fibers with tens of kilometers ranges [1], [2], [3], [4], [5], [6], so it is naturally suitable for large-scale and high-density sensing monitoring of IoT, such as production line monitoring, urban infrastructure monitoring, etc. Spatial resolution (SR) is one of the most important parameters of BOTDA sensors [7], [8], [9], [10], [11], representing the minimum fiber length required to separate two events accurately. Conventionally, the SR depends on the pulse width of the system. Since the lifetime of phonon in fiber is about 10 ns, when the pulse width is less than 10 ns, the incomplete excitation of phonon will lead to the broadening of Brillouin gain spectrum (BGS) and the considerable reduction of Brillouin gain, which will seriously affect the measurement accuracy of Brillouin frequency shift (BFS). As a result, the SR of BOTDA systems is usually larger than 1 m. But this is not enough for some applications where precise measurements of very short events are required, such as aircraft structure health monitoring, mine safety monitoring, etc., the temperature/strain variations in the submeter range must be accurately monitored. The motivation of the proposed work is to address one of the most critical technical bottlenecks in BOTDA sensors, i.e., improving the SR to submeter scale. However, the current research gap in BOTDA sensors is that there is hardly simple and convenient method to enhance the SR without hardware changes and distortion-free result. By now, various approaches have been proposed to enable submeter SR, such as the acoustic field pre-excitation technique. This technique pre-excites the acoustic field in the fiber by specially modulating the pump pulse. Various implementations have been proposed based on this principle, mainly, including pulse prepump (PPP) technique [12], dark-pulse technique [13], Brillouin echo distributed sensing (BEDS) technique [14], and Brillouin gain-profile tracing (GPT) technique [15]. However, most of these approaches require system

Manuscript received 5 February 2022; revised 20 May 2022, 27 July 2022, and 29 August 2022; accepted 21 September 2022. Date of publication 27 September 2022; date of current version 6 January 2023. This work was supported in part by the National Key Research and Development Program of China under Grant 2018YFB1801002; in part by the National Natural Science Foundation of China under Grant 61931010; in part by the Fundamental Research Funds for the Central Universities under Grant HUST: 2021XXJS026; in part by the Hubei Province Key Research and Development Programs under Grant 2020BAA006; and in part by the Innovation Fund of WNLO. (Zhao Ge and Li Shen contributed equally to this work.) (Corresponding authors: Hao Wu; Zhiyong Zhao.)

The authors are with the School of Optical and Electronic Information, Huazhong University of Science and Technology, Wuhan 430074, China (e-mail: m201977113@hust.edu.cn; shenli@hust.edu.cn; zhao_can@hust.edu.cn; wuhaoboom@qq.com; zhiyongzhao@hust.edu.cn; tangming@mail.hust.edu.cn).

Digital Object Identifier 10.1109/JIOT.2022.3209674

modification with complicated pulse modulation, which is thus generally more difficult to be implemented, and typically, the sensing distance is short. In addition to the acoustic field pre-excitation technique, another well-known scheme is the differential pulse-width pair (DPP) technique [16], [17], [18], [19], [20]. In DPP-BOTDA, two Brillouin time-domain traces are separately measured using two long pump pulses with a width difference, and high SR sensing signals can be obtained by subtracting the measured traces from each other. DPP-BOTDA has the advantages of easy implementation and long sensing distance, but it takes twice the measurement time and is more vulnerable to polarization fading noise and system instability [21]. Due to these drawbacks, it is necessary to explore new ways to obtain high SR directly from the measured BGS with long pump pulses, which can reduce the measurement time while improving the BFS accuracy.

Recently, signal post-processing methods have been proposed to achieve this purpose [22], [23], [24], which can significantly improve the SR by analyzing the BGS with specially designed algorithms. In the pump pulse subdivision method, the measurement results of a long pump pulse are considered as a superposition of several short pulses, and high SR can be retrieved by recovering the sensing signals related to the short pulse [24]. Another kind of method to improve SR is to use a deconvolution algorithm. By approximating the Brillouin time-domain traces as a linear convolution between pump pulse shape and fiber impulse response, the deconvolution algorithm successfully obtains a 0.2-m SR from the measured BGS with 40-ns pump pulse [21]. The advantages of the post-processing algorithm mainly include that no hardware changes are required and the SR is flexibly adjustable. Therefore, it shows much better improvement over the state-of-the-art techniques in terms of system complexity, measurement time, reliability, etc. However, because of the inertial features of the acoustic wave, BOTDA sensors cannot be rigorously regarded as a linear time-invariant system [21], [25]. Consequently, the Brillouin gain envelope is influenced by the detuned frequency along the fiber, and the above-mentioned post-processing methods will lead to notable distortions in the recovered results where BFS has a sharp and large change [21]. Although some sophisticated preprocessing methods have been proposed to eliminate this distortion, e.g., by using pulse differential preprocessing, it will however cause an increase of measurement time [25], [26].

With the development of artificial intelligence, neural networks are now increasingly applied in BOTDA sensors. In the past, neural network is generally used for denoising [27], extracting the BFS [2] (cannot improve the SR), and accelerating the data processing [28]. Experimental results have demonstrated that for BFS extract, convolutional neural network (CNN) outperforms the traditional Lorentz curve fitting (LCF) method in both precision and computation speed [2], [29]. These results show that CNN has a 2-D feature extraction ability and nonlinear mapping function, which can comprehensively analyze the features of BGS over a certain length of fiber to acquire the BFS distribution. Therefore, it is expected that the outstanding performance of CNN might also find application in enabling high SR measurement

in BOTDA sensors, where CNN may have the capacity to directly achieve high SR by matching the BGS features to the BFS distribution, and avoid distortion caused by conventional post-processing methods.

To overcome the disadvantages of traditional schemes, a deep learning algorithm based on CNN is proposed to improve the SR of conventional BOTDA sensors in this work. Therefore, the objective of this work is to develop a novel high SR distributed fiber optic sensing algorithm for high precision infrastructure structure monitoring systems. To train the CNN, a large number of BGSs is simulated as the CNN input training data, and the corresponding high SR BFS distribution is used as the CNN output target. After the training, simulation results indicate that the CNN can realize precise BFS extraction with high SR from the input BGS that is generated by a long pulse. In the experiment, the CNN can accurately recover the 0.5-m SR BFS distribution when 20–50 ns pump pulses are used, and the obtained BFS is in great agreement with the 45/40 ns DPP measurement results. By changing the simulated training data sets, variable high SR sensing information can be recovered directly from measured BGS with different long pump pulse widths. To our knowledge, the proposed CNN-based high SR retrieval scheme has not been reported before, therefore, this work is of great significance.

The main contributions of our scheme can be summarized as follows.

- 1) *Novel High SR Measurement Method for BOTDA Sensors:* Limited by the acoustic lifetime, the SR of conventional BOTDA sensors is restricted to be longer than 1 m. This does not meet the needs of many applications. The proposed deep-learning-based technique in this work paves the way to enable a novel high SR measurement method for BOTDA sensors.
- 2) *CNN-Based High SR Retrieval Technique:* The CNN-based high SR retrieval technique is proposed to directly retrieve the accurate BFS distribution with much higher SR from the measured BGS that is acquired by using a long pump pulse. So far, the conventional high SR BOTDA technologies mainly includes acoustic field pre-excitation technology, pulse differential technology, and signal post-processing technology. To our knowledge, this is the first time to propose the BFS retrieval with submeter SR by CNN. Compared with the conventional schemes, the proposed method has the advantages of shorter measurement times, no distortion in the measurement results, lower measurement uncertainty, and no hardware modifications.
- 3) *Performance Evaluation of the CNN-Based High SR Retrieval Algorithm:* We have studied thoroughly the effectiveness of the CNN-based high SR retrieval algorithm based on the simulation testset, experimental testset, the standard deviation of measurement, and uncertainty of measurement. Excellent feasibility of the proposed data processing algorithm is verified. It is believed that the proposed technology will benefit a lot for IoT on high precision monitoring of infrastructures.

In this article, a CNN algorithm-based SR improvement approach is proposed. Section II will introduce the architecture

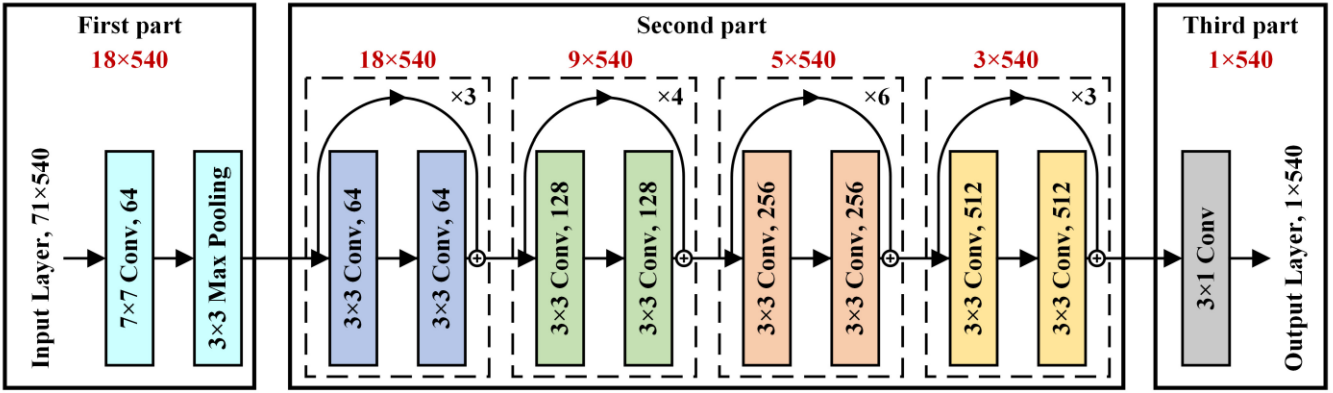


Fig. 1. Architecture of the proposed CNN.

of the proposed CNN, including its composition, parameters, and function. Section III will present the investigation of simulation, including the generation of simulation data, the training, and verification of the simulation model. Section IV will present the experimental results, including the CNN processed result and its comparison with the result of conventional DPP scheme. In addition, the results of high SR retrieval from different pulse widths will also be presented. Finally, a conclusion will be given in Section V.

II. ARCHITECTURE OF THE PROPOSED CNN

CNN is one of the representative algorithms of deep learning, which is generally composed of convolution, pooling, and full connected layers. But in this article, the full connection layer is replaced by the convolution layer. Thus, CNN can accurately identify the BFS change with a length lower than the SR and locate the position of the change point. In BOTDA sensing, when there are multiple BFS variation regions within the SR length of the fiber, each BGS curve is affected by the true BFS (labeled values) in its surrounding SR range. Therefore, in order to enable the CNN to recognize cm-level BFS changes, the convolutional layers must be deep enough to ensure that the lateral receptive field covers more than one SR length. However, deep CNNs suffer from gradient disappearance and network degradation [30], and the residual module of ResNet is a good solution to this problem [30]. On the other hand, it has been demonstrated that the residual module can help to obtain the distributed BFS directly from the measured 2-D BGS [2], which shows that the ResNet has excellent potential for BFS feature extraction.

As shown in Fig. 1, the structure of the proposed CNN consists of three parts, with a total of 34 convolutional layers and one pooling layer. The first part mainly includes an input layer, a convolutional (Conv) layer with 64 filters of size 7×7 and a maximum pooling layer with 64 filters of size 3×3 . The input layer is used for the import of BGS. The size of input data is 71×540 , where the height 71 is the number of swept frequencies of the BGS, and the width 540 is the number of BGS along the fiber length direction. By carefully designing the stride length and padding size of the convolutional and pooling layers, as marked by the red numbers in Fig. 1, the size of the 64 output feature maps

after the first part is reduced to 18×540 , which can greatly reduce the number of unnecessary parameters in the CNN. To alleviate the internal covariate shift problem and add nonlinear factors, batch-normalization (BN) layer and rectified linear unit (ReLU) activation function are also contained in the first part [31], [32].

The second part of the CNN is a deep neural network to extract the features of the BGS, which is composed of 16 residual blocks to ensure a large enough receptive field covering the BGS with length longer than the pump pulse width [30], [33]. Each residual block has two convolutional layers, BN layers, and ReLU activation function, and there is a shortcut connection between the input and output to solve the vanishing gradients and degradation problems of deep neural networks [28]. According to the number of filters in the convolutional layers, the 16 residual blocks can be divided into four categories with 64, 128, 256, and 512 filters, and the numbers of residual blocks in each category are 3, 4, 6, and 3, respectively. As indicated by the red numbers in Fig. 1, during the CNN processing, the size of output feature maps after each network section gradually decreases in the frequency direction but remains unchanged in the fiber length direction.

The third part of the CNN is a single convolutional layer aims to traverse the data to the 1-D BFS distribution.

The final output size of the CNN is 1×540 , which is the BFS corresponding to each input BGS, thereby accomplishing the BFS extraction task.

III. SIMULATION RESULTS

A. Simulation Data-Generation

To make the CNN has an accurate BFS determination ability for various application situations, a large amount of training data is required, which is all generated by the mathematical model in this work. In the simulation, the BGS of a 54-m fiber is calculated, which is composed of multiple uniform fiber sections with lengths from 0.5 to 5 m. As listed in Table I, the BFS, section length, normalized gain intensity, and intrinsic Brillouin linewidth of each uniform section are set with random distributed values. Thus, the obtained BGS contains various situations. It is presumed that the shortest

TABLE I
RANDOM RANGES OF SIMULATION PARAMETERS

Parameters	Random Range
BFS	10.81–10.89 GHz
Length of Fiber Sections	0.5–5 m
Normalized Gain Intensity	0.8–1
Intrinsic Brillouin Linewidth	25–35 MHz

length of uniform fiber sections has an important impact on the CNN, because it represents the minimum length of BFS change that the CNN can be applied to after the training, i.e., the SR of the system. According to the uniform fiber sections ranges, the expected SR of the trained CNN is 0.5 m. Considering that the Brillouin gain intensity is affected by temperature and strain change, the normalized gain intensity fluctuates between 0.8 and 1. The change of Brillouin gain intensity is approximately linear with strain and temperature, and the intensity decreases with decreasing temperature and increasing strain [34]. It is worth mentioning that the linewidth in Table I is the intrinsic Brillouin linewidth, and the simulated BGS linewidth is also related to the pump pulse width, which will be broader when narrow pump pulse is used [35].

With the given simulation parameters, the BGS at fiber position z can be solved by the concatenation of Brillouin gain of lots of very short fiber unit within the pump pulse width, which can be calculated by [36], [37]

$$a_s(z) = \sum_{N=0}^{l/\Delta z} a_s^{\text{short}}\left(z - N\Delta z, \frac{z + N\Delta z}{V_g}\right) \quad (1)$$

where l is the length of pump pulse, Δz is the length of a short fiber unit, which is 1 cm in the simulation, and a_s^{short} is the generated Brillouin gain of one fiber unit, which can be expressed as [36], [37]

$$a_s^{\text{short}}(z, t) = g(z) \frac{I_P^0 A_S^0}{2\Gamma_A^*} \Delta z \left\{ 1 - \exp \left[-\Gamma_A^* \left(t - \frac{z + \Delta z}{V_g} \right) \right] \right\} \\ \left[u \left(t - \frac{z + \Delta z}{V_g} \right) - u \left(t - T - \frac{z + \Delta z}{V_g} \right) \right] \quad (2)$$

where $a_s^{\text{short}}(z, t)$ is the Brillouin gain at position z and time t , $g(z)$ is a constant related to the electrostrictive constant, I_P^0 and A_S^0 are the pump pulse and constant acoustic wave intensity, respectively, V_g is the light velocity in the fiber, u is the heaviside unit step function, T is the pump pulse width, and $\Gamma_A = i\pi(v_B^2(z) - v^2 - iv_B)$ is the frequency detuning parameter, where v_B and v are the BFS at position z and the sweep frequency, respectively, and $\Delta\nu_B$ is the intrinsic Brillouin linewidth [32]. The BGS is simulated with a rectangular 40-ns pump pulse and sampling rate of 1 GSa/s. The frequency sweep range is 10.78–10.92 GHz with a step of 2 MHz to obtain a total of 71 frequencies. It should be pointed out that this also determines the scanning frequency number in the experiments, so as to ensure that the trained network is applicable to the experimentally collected BGS data. Then, the obtained BGS is divided into size of 71×540

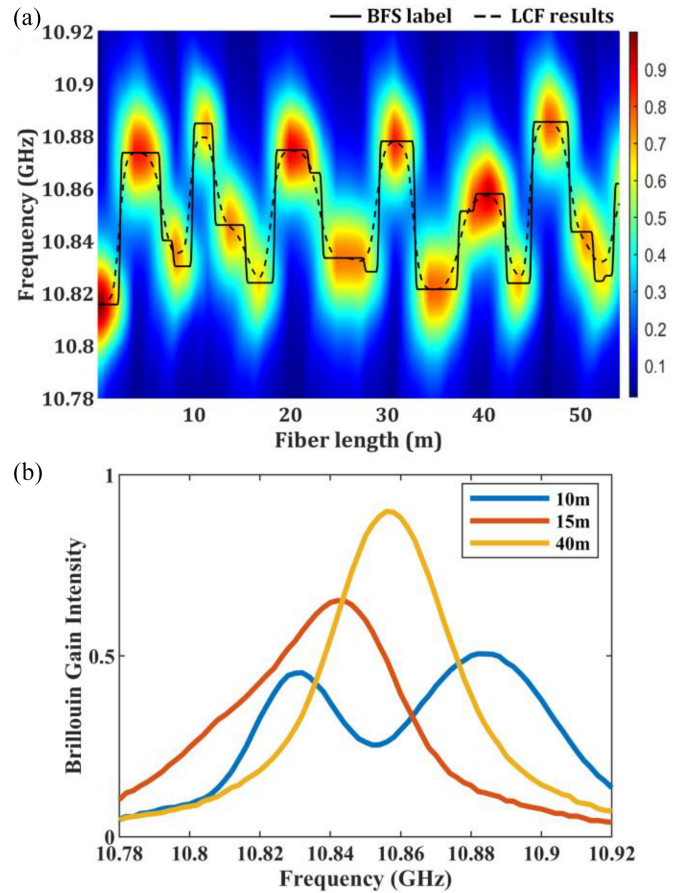


Fig. 2. Simulated BGS as a function of fiber length and the corresponding BGS at 10, 15, and 40 m, respectively.

and normalized according to the maximum Brillouin gain. It is worth noting that the width number needs to be chosen to make sure its size is larger than the sampling points that are determined by the system's SR. Finally, Gaussian white noise is added to the normalized BGS with random variance between 0.005 and 0.0005, resulting in an SNR between 23 and 33 dB.

On the other hand, as the CNN output target, the corresponding BFS label also needs to be normalized by

$$\text{BFS}_N = \frac{\text{BFS} - \text{BFS}_{\min}}{\text{BFS}_{\max} - \text{BFS}_{\min}} \quad (3)$$

where BFS_N is the BFS after normalization, which varies between 0 and 1, and BFS_{\max} and BFS_{\min} are the maximum and minimum values of the BFS range, respectively. Meanwhile, to make the BFS label has a 0.5-m SR as well, a Gaussian filter is applied to the BFS to generate smooth rising/falling edges. It is very important that the bandwidth of the Gaussian filter should not degraded the SR worse than 0.5 m. So, a Gaussian filter with 200-MHz bandwidth is used in the simulation, which corresponds to an SR of 0.5 m exactly [38], [39]. It should be noted that although filtered BFS label allows the CNN to obtain a more stable prediction at the BFS changing regions, the rising/falling length will be longer.

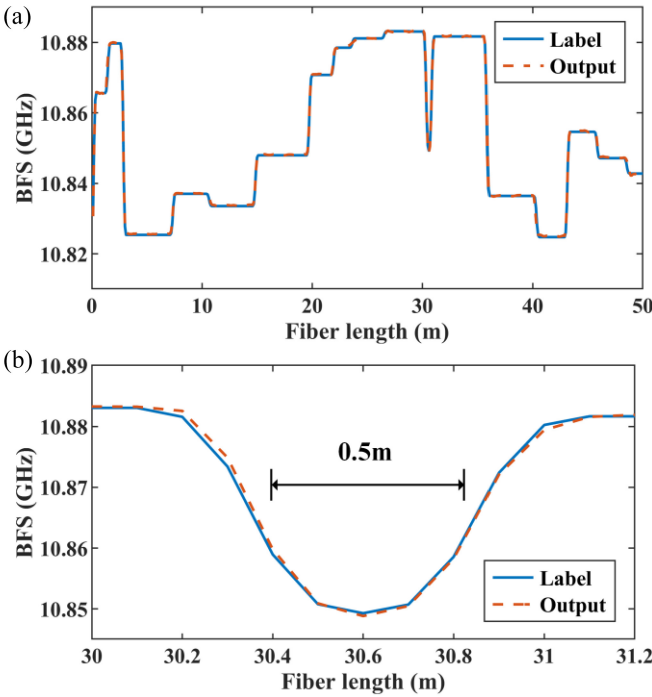


Fig. 3. (a) Comparation between BFS label and CNN output results. (b) BFS label and CNN output results at 0.5-m changing region.

B. Simulation Verification of the CNN

In the simulation, 10 000 sets of training data were generated, and 2000 sets of validation data were generated, the size of each data is 71×540 , one of which is shown in Fig. 2, where the solid line is the BFS label. We can observe that since the pump pulse width in the simulation is 40 ns, the BGS of uniform fiber sections that is shorter than 4 m will be distorted due to SR limitation. As an example, Fig. 2(b) shows the comparison between the distorted and undistorted BGS. It is observed that the Brillouin gain curve at 10 m is affected by severe nonlocal distortion due to insufficient SR, where the Brillouin gain curve has two peaks, stemming from the superposition of nonlocal gain spectrums. As shown by the dashed line of LCF results in Fig. 2(a), accurate BFS cannot be acquired for these distorted regions. Different from the principle of LCF which only analyzes the BGS at single fiber location, with the multilayer convolutional structure, the predicted BFS of CNN at every location is based on the features of BGS in the receptive field. Although the original SR of input BGS is limited by pump pulse width, during the training process, the CNN is automatically learned to recover a BFS distribution that best fits the output label, which has an SR of 0.5 m. Thus, the trained CNN can achieve higher SR from a measured BGS with long pump pulses.

During the training, the CNN is initialized with the Kaiming method. Adam optimization is employed to minimize the mean squared error (MSE) loss function with a learning rate of 10^{-4} . The batch size is 12, which is limited by GPU. During the training, the model first predicts the BFS of the training set by forward-propagation, then calculates the loss value with the prediction results and labels, and then back propagates the loss, after which the parameters of the network are

updated to minimize the loss. If all the data in the training set are processed through the whole procedure, one epoch is completed. At the end of each epoch, the validation set is fed to the newly generated model to calculate the validation loss. The epoch with the smallest MSE in the validation set will be selected as the optimal model, and training is stopped when the optimal model remains unchanged for 50 consecutive epochs. In our experiment, after training the CNN for 82 epochs, the optimal model is obtained with an MSE loss of 9.93×10^{-5} . It requires about 7.7 h to complete the training with an NVIDIA TITAN RTX GPU.

The SR used in the experiments is 4 m, and the sampling rate is 1 GS/s, so each BGS curve is jointly affected by the surrounding 40 real BFSs around it considering the sampling period of 0.1 m. In the experiments, the size of the BFS output from our model is 1×540 . However, it is worth mentioning that the edge region of the BGS is also related to the BFS outside the processed BGS spectrum, therefore, the BFS around the edge region of the BGS may not be retrieved precisely. So only the output with the center size of 1×500 is used to obtain an accurate MSE loss. The measured BGS is divided into multiple sections with overlapping areas in the experiment. The CNN only needs to focus on retrieving the true BFS in the center part.

To evaluate the performance of the trained CNN, a test data set is generated in the same way as the training data set. There are 2364 sets of data in the simulation test set, and the size of each data is 71×540 . The blue line and red dashed line in Fig. 3(a) show the comparison of BFS label and CNN output, respectively. It can be discovered that there is no apparent error, and the output results are consistent with the label. The standard deviation of the prediction error for all samples in the test set is 0.65 MHz. For the BFS changing regions with 0.5-m length, as shown in Fig. 3(b), the CNN can accurately extract the BFS distribution without obvious distortion, which proves that the CNN has an SR of 0.5 m. In addition, the SR of this CNN can be flexibly adjusted by changing the training data set with different target SR.

It is worth noting that the purpose of the simulation is to train a CNN that can recognize 0.5-m SR. Without Gaussian filtering, the simulated BFS trace has a sharp rising/falling edge of 0.1 m, much higher than the targeted 0.5-m SR. This makes it difficult for CNN to accurately predict the position of the rising/falling edge of BFS, which may lead to an apparent incorrect retrieval, as shown by the blue line and red dashed line in Fig. 4. To reduce this prediction error, a Gaussian filter is applied to the BFS trace of the training data set to generate a smoother label as the yellow line shown in Fig. 4, thus, facilitating the CNN better to learn the characteristics of the changing regions of BFS trace. It is very important that the bandwidth of the Gaussian filter should be carefully chosen to avoid degrading the SR. A Gaussian filter with 200-MHz bandwidth is used in the simulation, corresponding to 0.5-m rising/falling edge, which is the same as the minimum SR to be recovered. After training with the filtered BFS, the CNN prediction result is shown by the purple lines in Fig. 4. We can observe that the CNN predicted trace is smoother, and there is no apparent incorrect retrieval between

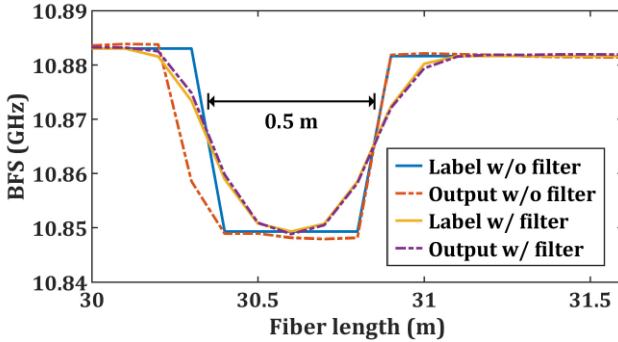


Fig. 4. Comparation between CNN output and corresponding label with and without Gaussian filter applied to the BFS of the training data set.

the CNN prediction and BFS labels for the 0.5-m change area. Simulation results indicate that the standard deviation of prediction error is reduced from 1.95 to 0.65 MHz by training with the filtered BFS.

IV. EXPERIMENTAL SETUP AND RESULTS

To further verify the effect of the CNN, a typical BOTDA sensor as shown in Fig. 5 is used to measure the experimental data. The continuous wave light output from the laser source is divided into probe and pump light by a 50:50 optical coupler. The probe light on the upper branch is modulated by an electro-optical modulator (EOM) to sweep the frequency, which is driven by a radio frequency (RF) generator through carrier-suppressed double-sideband modulation. And the sweep range is 10.81–10.89 GHz in 2-MHz steps. The probe light is finally launched into the 4.9-km long sensing fiber through an isolator. There are three hotspots placed at the end of the fiber, with lengths of 3.3, 1, and 0.5 m, respectively. The lower branch is used for pump light which is modulated by another EOM to generate high extinction ratio pump pulse with fast rising/falling time by using a programmable electrical pulse generator. The erbium-doped fiber amplifier (EDFA) is used to amplify the pump pulse light, and then, the amplified pump pulse light passes through a polarization switch (PS) to reduce the polarization fading noise of the Brillouin gain. At the receiver side, a fiber Bragg grating (FBG) is employed to reflect the Brillouin Stokes sideband. The Brillouin signal is finally detected by a photodetector (PD) and then acquired and displayed on an oscilloscope.

A 40-ns pump pulse is used in the experiment as in the simulation, and the sampling rate is 1 GSa/s. The SNR of the experimental raw data is about 25.8 dB. As shown by the blue line in Fig. 6, LCF is used for the obtained BGS, which has a theoretical SR of 4 m. We can discover that the hotspots cannot be accurately measured. Then, the experimental data are processed by the trained CNN, and the output BFS distribution near the hotspots are shown as the green dashed line. Finally, a 45/40-ns DPP is performed, and the red line shows the obtained BFS distribution as a reference. The comparison results indicate that the CNN can accurately retrieve the BFS of the hotspots, and the recovered result is in great agreement with the 45/40-ns DPP. Fig. 6(b) is an enlarged view of the

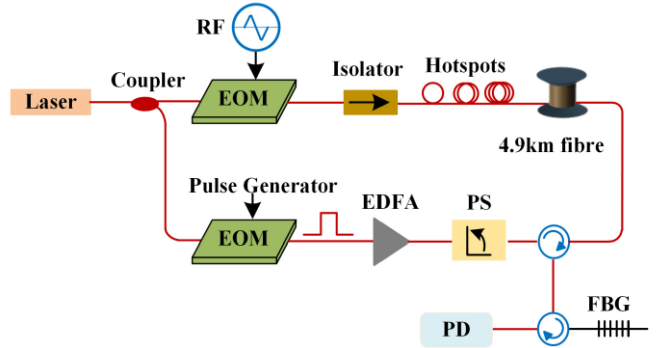


Fig. 5. Experimental setup of the BOTDA system. RF: radio frequency, EOM: electro-optic modulator, PS: polarization switch, EDFA: erbium-doped fiber amplifier, FBG: fiber Bragg grating, PD: photodetector..

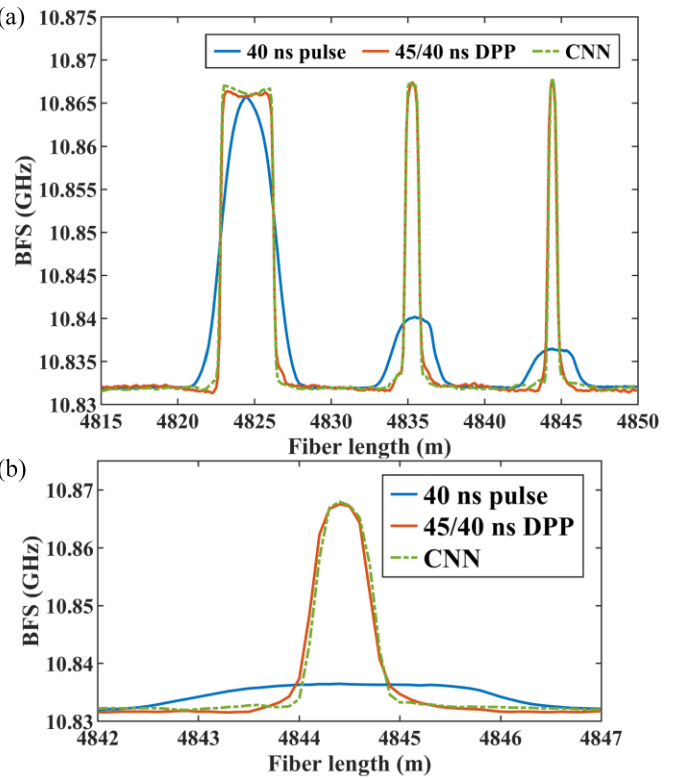


Fig. 6. (a) 40-ns pump pulse measurement results in the experiment. (b) Enlarged view of 0.5-m hotspot.

0.5-m hotspot in Fig. 6(a). The maximal error between CNN prediction and DPP calculation is only 0.4 MHz in Fig. 6(b).

BFS uncertainty is then compared to quantify the performance of the CNN. We performed a total of six experiments and calculated the uncertainty of the 45/40-ns DPP method's results and the CNN method's results for these six experiments. The calculated BFS standard deviation of the six measurements is regarded as BFS uncertainty, shown in Fig. 7. The uncertainty of the 45/40-ns DPP and the CNN is shown by the blue and red lines, respectively. The quadratic fitting of the uncertainty results from the two methods is shown by the yellow and purple dotted lines, respectively. Under the same SR of 0.5 m, the average uncertainty of CNN prediction along the fiber is 0.31 MHz, which is only half of the 45/40-ns DPP. In addition, compared with the DPP

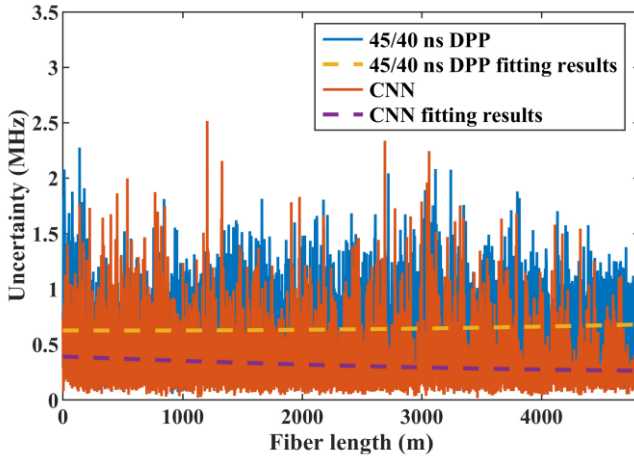


Fig. 7. BFS uncertainty comparation between DPP and CNN for the experimental results.

technique, by avoiding the signal differential process, the CNN reduces the required measurement time by half. Additionally, based on the python environment on the same computer, CNN only needs about 0.14 s to process 10 000 BGS, while the traditional LCF used in DPP system needs 7.3 s. These results indicate that the proposed high SR BFS retrieval method with CNN has the advantages of short measurement time and fast processing speed, which shows substantial improvement over the state-of-the-art techniques in terms of system complexity, measurement time, reliability, etc.

Eventually, to make the CNN applicable to various pump pulse widths, training data sets were also simulated with 20, 30, and 50 ns pump pulses to generate multiple CNN models. And the performance of these models was verified using the experimental data measured with corresponding pump pulse widths. The results are all shown in Fig. 8. For pump pulse widths between 20 and 50 ns, the obtained BFSs have a good consistency, and the average uncertainty between different pump pulse widths is 0.63 MHz. These experimental results indicate that the CNN can be applied to different pump pulse widths by using matched training data. In addition, it is worth mentioning that by changing the training data sets with different targeted SR, the trained CNNs can achieve variable high SR retrieval from a long pulse BOTDA sensor. The unprecedented adjustable capability of SR enabled in software shows much better flexibility than the traditional approaches requiring hardware modification.

V. CONCLUSION

In this article, we present a novel high SR distributed fiber optic sensing algorithm for a high-precision infrastructure structure monitoring system on the IoT. To realize the proposed algorithm, a CNN is proposed to directly retrieve the accurate BFS distribution with much higher SR from the measured BGS that is acquired by using a long pump pulse. In the experiment, 0.5-m SR is successfully obtained with long pump pulses from 20 to 50 ns, and the CNN processed results are in good agreement with the 45/40-ns DPP measurement result, which verifies the excellent feasibility of the

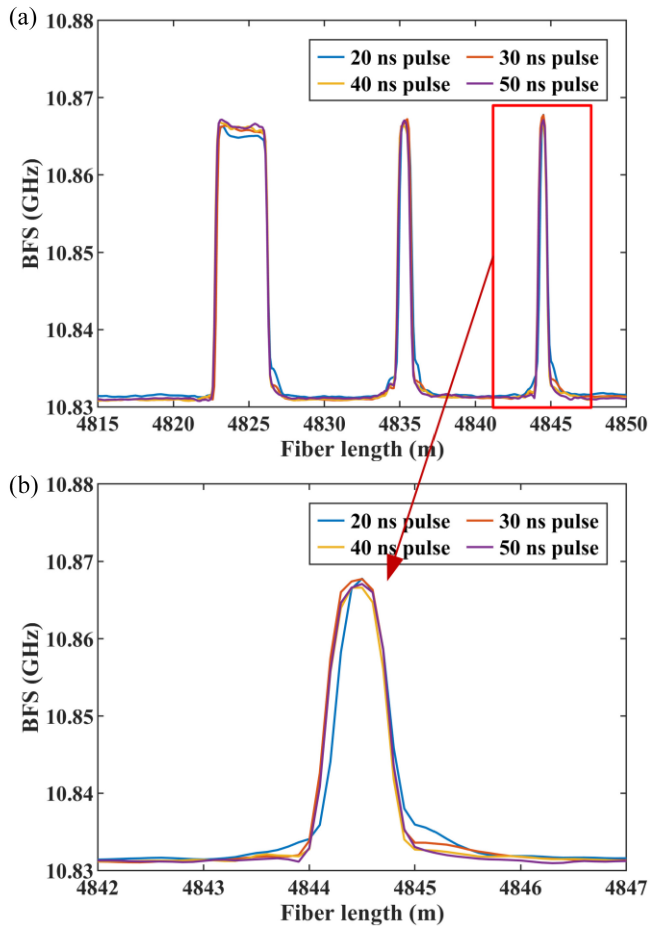


Fig. 8. (a) BFSs retrieved by CNNs from different pump pulse widths between 20 and 50 ns. (b) Enlarged view of 0.5-m hotspot.

proposed high-SR algorithm. Under the same SR, the proposed algorithm shows a twofold improvement in BFS uncertainty over the DPP technique and consumes only half the measurement time. By designing the training data sets, the proposed algorithm with variable SR can be widely used in traditional BOTDA systems to improve the SR without the requirement of hardware modification. To our knowledge, this is the first time to propose such an approach, i.e., submeter scale SR enhancement by using CNN, and the feasibility has been experimentally validated fully. The proposed technique in this work paves the way to enable a novel high SR measurement method for BOTDA sensors, which shows unprecedented improvement over the state-of-the-art techniques in terms of system complexity, measurement time, reliability, etc.

Future work will focus on improving the performance of such a sensing system, particularly to achieve more flexible and fast adjustment of SR, which is quite important in practical applications. However, adjusting the SR requires the corresponding adjustment of the data in the training set and retraining, which consumes a lot of time and computational resources. In order to solve this problem, transfer learning will be used, which is to apply the CNN model trained on one task to another similar task through simple adjustment. Compared with the traditional learning procedures, transfer learning can shorten the training time, improve the model's recognition

performance, and offer better fitting accuracy. Therefore, it is necessary to explore transfer learning methods to realize fast network switching and thus reducing the training time.

REFERENCES

- [1] T. Horiguchi, T. Kurashima, and M. Tateda, "A technique to measure distributed strain in optical fibers," *IEEE Photon. Technol. Lett.*, vol. 2, no. 5, pp. 352–354, May 1990.
- [2] Y. Chang, H. Wu, C. Zhao, L. Shen, S. Fu, and M. Tang, "Distributed Brillouin frequency shift extraction via a convolutional neural network," *Photon. Res.*, vol. 8, no. 5, pp. 690–697, Apr. 2020.
- [3] T. Kurashima, T. Horiguchi, and M. Tateda, "Distributed-temperature sensing using stimulated Brillouin scattering in optical silica fibers," *Opt. Lett.*, vol. 15, no. 18, pp. 1038–1040, Sep. 1990.
- [4] M. A. Soto, J. A. Ramírez, and L. Thévenaz, "Intensifying the response of distributed optical fibre sensors using 2-D and 3D image restoration," *Nat. Commun.*, vol. 7, no. 1, pp. 1–11, Mar. 2016.
- [5] B. Wang, D. Ba, Q. Chu, L. Qiu, D. Zhou, and Y. Dong, "High-sensitivity distributed dynamic strain sensing by combining Rayleigh and Brillouin scattering," *Opto-Electron. Adv.*, vol. 3, no. 12, pp. 1–8, Dec. 2020.
- [6] Z. Zhao, M. Tang, and C. Lu, "Distributed multicore fiber sensors," *Opto-Electron. Adv.*, vol. 3, no. 2, Mar. 2020, Art. no. 190024.
- [7] M. Luo, J. Liu, C. Tang, X. Wang, T. Lan, and B. Kan, "0.5 mm spatial resolution distributed fiber temperature and strain sensor with position-deviation compensation based on OFDR," *Opt. Exp.*, vol. 27, no. 24, pp. 35823–35829, Nov. 2019.
- [8] J. Li *et al.*, "High spatial resolution distributed fiber strain sensor based on phase-OFDR," *Opt. Exp.*, vol. 25, no. 22, pp. 27913–27922, Oct. 2017.
- [9] B. Lu *et al.*, "High spatial resolution phase-sensitive optical time domain reflectometer with a frequency-swept pulse," *Opt. Lett.*, vol. 42, no. 3, pp. 391–394, Jan. 2017.
- [10] Y. Liu, L. Ma, C. Yang, W. Tong, and Z. He, "Long-range Raman distributed temperature sensor with high spatial and temperature resolution using graded-index few-mode fiber," *Opt. Exp.*, vol. 26, no. 16, pp. 20562–20571, Aug. 2018.
- [11] Z. Liang *et al.*, "Spatial resolution improvement of single-shot digital optical frequency comb-based Brillouin optical time domain analysis utilizing multiple pump pulses," *Opt. Lett.*, vol. 43, no. 15, pp. 3534–3537, Jul. 2018.
- [12] K. Kishida, C.-H. Li, and K. I. Nishiguchi, "Pulse pre-pump method for cm-order spatial resolution of BOTDA," in *Proc. 17th Int. Conf. Opt. Fibre Sens.*, Bruges, Belgium, 2005, pp. 559–562.
- [13] A. W. Brown, B. G. Colpitts, and K. Brown, "Distributed sensor based on dark-pulse Brillouin scattering," *IEEE Photon. Technol. Lett.*, vol. 17, no. 7, pp. 1501–1503, Jul. 2005.
- [14] D. D. Sampson, L. Thévenaz, and S. F. Mafang, "Distributed fiber sensing using Brillouin echoes," in *Proc. 19th Int. Conf. Opt. Fibre Sens.*, Perth, WA, Australia, 2008, Art. no. 70043N.
- [15] T. Sperber, A. Eyal, M. Tur, and L. Thévenaz, "High spatial resolution distributed sensing in optical fibers by Brillouin gain-profile tracing," *Opt. Exp.*, vol. 18, no. 8, pp. 8671–8679, Apr. 2010.
- [16] S. Diakaridisa *et al.*, "Detecting cm-scale hot spot over 24-km-long single-mode fiber by using differential pulse pair BOTDA based on double-peak spectrum," *Opt. Exp.*, vol. 25, no. 15, pp. 17727–17736, Jul. 2017.
- [17] W. Li, X. Bao, Y. Li, and L. Chen, "Differential pulse-width pair BOTDA for high spatial resolution sensing," *Opt. Exp.*, vol. 16, no. 26, pp. 21616–21625, Dec. 2008.
- [18] A. Minardo, R. Bernini, and L. Zeni, "Numerical analysis of single pulse and differential pulse-width pair BOTDA systems in the high spatial resolution regime," *Opt. Exp.*, vol. 19, no. 20, pp. 19233–19244, Sep. 2011.
- [19] J. Urricelqui, M. Sagues, and A. Loayssa, "Phasorial differential pulse-width pair technique for long-range Brillouin optical time-domain analysis sensors," *Opt. Exp.*, vol. 22, no. 14, pp. 17403–17408, Jul. 2014.
- [20] H. Wu, L. Wang, Z. Zhao, C. Shu, and C. Lu, "Support vector machine based differential pulse-width pair Brillouin optical time domain analyzer," *IEEE Photon. J.*, vol. 10, no. 4, pp. 1–11, Aug. 2018.
- [21] S. Wang, Z. Yang, S. Zaslawski, and L. Thévenaz, "Short spatial resolution retrieval from a long pulse Brillouin optical time-domain analysis trace," *Opt. Lett.*, vol. 45, no. 15, pp. 4152–4155, Jun. 2020.
- [22] R. Bernini, A. Minardo, and L. Zeni, "Accuracy enhancement in Brillouin distributed fiber-optic temperature sensors using signal processing techniques," *IEEE Photon. Technol. Lett.*, vol. 16, no. 4, pp. 1143–1145, Apr. 2004, doi: [10.1109/LPT.2004.824982](https://doi.org/10.1109/LPT.2004.824982).
- [23] F. Wang, W. Zhan, X. Zhang, and Y. Lu, "Improvement of spatial resolution for BOTDR by iterative subdivision method," *J. Lightw. Technol.*, vol. 31, no. 23, pp. 3663–3667, Dec. 2013, doi: [10.1109/JLT.2013.2286193](https://doi.org/10.1109/JLT.2013.2286193).
- [24] J. Chao, X. Wen, W. Zhu, L. Min, H. Lv, and S. Kai, "Subdivision of Brillouin gain spectrum to improve the spatial resolution of a BOTDA system," *Appl. Opt.*, vol. 58, no. 2, pp. 466–472, 2019.
- [25] L. Shen, Z. Zhao, C. Zhao, H. Wu, C. Lu, and M. Tang, "Improving the spatial resolution of a BOTDA sensor using deconvolution algorithm," *J. Lightw. Technol.*, vol. 39, no. 7, pp. 2215–2222, Apr. 1, 2021, doi: [10.1109/JLT.2020.3047504](https://doi.org/10.1109/JLT.2020.3047504).
- [26] W. Wei, L. Shen, Z. Zhao, C. Zhao, and M. Tang, "Performance enhanced BOTDA sensor using differential Golay coding and deconvolution algorithm," in *Proc. Opt. Fiber Commun. Conf. Exhibition*, San Francisco, CA, USA, 2022, pp. 1–3.
- [27] H. Wu *et al.*, "Real-time denoising of Brillouin optical time domain analyzer with high data fidelity using convolutional neural networks," *J. Lightw. Technol.*, vol. 37, no. 11, pp. 2648–2653, Jun. 1, 2019.
- [28] N. Lalam, A. Venkateswaran, P. Lu, and M. Buric, "Probabilistic deep neural network based signal processing for Brillouin gain and phase spectrums of vector BOTDA system," in *Proc. Opt. Interconnects XXI*, 2021, Art. no. 11692.
- [29] D. Qi, J. Li, X. Guan, and C. Chan, "Dynamic polarization-insensitive BOTDA in direct-detection OFDM with CNN-based BFS extraction," *Opt. Exp.*, vol. 30, no. 5, pp. 7725–7736, Feb. 2022.
- [30] K. He, X. Zhang, S. Ren, and J. Sun, "Deep residual learning for image recognition," in *Proc. IEEE Conf. Comput. Vis. Pattern Recognit.*, Las Vegas, CA, USA, 2016, pp. 770–778.
- [31] S. Ioffe and C. Szegedy, "Batch normalization: Accelerating deep network training by reducing internal covariate shift," in *Proc. 32nd Int. Conf. Mach. Learn.*, Lille, France, 2015, pp. 448–456.
- [32] A. Krizhevsky, I. Sutskever, and G. E. Hinton, "ImageNet classification with deep convolutional neural networks," *Commun. ACM*, vol. 60, no. 6, pp. 84–90, Jun. 2017.
- [33] W. Luo, Y. Li, R. Urtasun, and R. Zemel, "Understanding the effective receptive field in deep convolutional neural networks," in *Proc. 30th Int. Conf. Neural Inf. Process. Syst.*, 2016, pp. 4905–4913.
- [34] M. Nikles, L. Thevenaz, and P. A. Robert, "Brillouin gain spectrum characterization in single-mode optical fibers," *J. Lightw. Technol.*, vol. 15, no. 10, pp. 1842–1851, Oct. 1997.
- [35] M. Alem, M. A. Soto, M. Tur, and L. Thévenaz, "Analytical expression and experimental validation of the Brillouin gain spectral broadening at any sensing spatial resolution," in *Proc. 25th Opt. Fiber Sens. Conf.*, 2017, pp. 1–4.
- [36] X. Sun *et al.*, "Frequency shift estimation technique near the hotspot in BOTDA sensor," *Opt. Exp.*, vol. 27, no. 9, pp. 12899–12913, Apr. 2019.
- [37] J.-C. Beugnot, M. Tur, S. F. Mafang, and L. Thévenaz, "Distributed Brillouin sensing with sub-meter spatial resolution: Modeling and processing," *Opt. Exp.*, vol. 19, no. 8, pp. 7381–7397, Apr. 2011.
- [38] X. Sun *et al.*, "Genetic-optimised aperiodic code for distributed optical fibre sensors," *Nat. Commun.*, vol. 11, no. 1, pp. 1–11, 2020.
- [39] S. Zaslawski, Z. Yang, and L. Thévenaz, "On the 2-D post-processing of Brillouin optical time-domain analysis," *J. Lightw. Technol.*, vol. 38, no. 14, pp. 3723–3736, Jul. 15, 2020.

Zhao Ge received the B.S. degree from the School of Physics and Information Engineering, Jianghan University, Wuhan, China, in 2019. He is currently pursuing the M.D. degree with the School of Optical and Electronic Information, Huazhong University of Science and Technology, Wuhan.

His research interests are optical fiber sensing and optical fiber devices.

Li Shen received the B.S. degree from the School of Optical and Electronic Information, Huazhong University of Science and Technology, Wuhan, China, in 2016, where he is currently pursuing the Ph.D. degree.

His research interests are optical fiber sensing and optical fiber devices.

Can Zhao received the B.S. and Ph.D. degrees from the School of Optical and Electronic Information, Huazhong University of Science and Technology (HUST), Wuhan, China, in 2014 and 2019, respectively.

He has been a Postdoctoral Researcher with HUST since 2019. His current research interests include distributed optical fiber sensing and specialty optical fiber.

Hao Wu received the B.S., M.Eng., and Ph.D. degrees from the School of Optical and Electronic Information, Huazhong University of Science and Technology (HUST), Wuhan, China, in 2013, 2016, and 2019, respectively.

He has been a Postdoctoral Researcher with HUST since 2019. His current research interests include the application of specialty optical fiber and machine learning algorithm in distributed optical fiber sensing.

Zhiyong Zhao (Member, IEEE) received the B.Eng. and Ph.D. degrees from Huazhong University of Science and Technology, Wuhan, China, in 2012 and 2017, respectively.

He was a joint Ph.D. student with the École polytechnique fédérale de Lausanne, Lausanne, Switzerland, from October 2014 to October 2015. In 2016, he was a Research Assistant with the School of Electrical and Electronic Engineering, Nanyang Technological University, Singapore. From June 2017 to October 2020, he was a Postdoctoral Fellow with the Department of Electronic and Information Engineering, Hong Kong Polytechnic University, Hong Kong. Since October 2020, he has been an Associate Professor with the School of Optical and Electronic Information, Huazhong University of Science and Technology. His current research interests include optical fiber sensing, optical fiber devices, special optical fibers, and nonlinear fiber optics.

Ming Tang (Senior Member, IEEE) received the B.E. degree from Huazhong University of Science and Technology (HUST), Wuhan, China, in 2001, and the Ph.D. degree from Nanyang Technological University, Singapore, in 2005.

His postdoctoral research with the Network Technology Research Centre, Nanyang Technological University was focused on optical fiber amplifiers, high-power fiber lasers, nonlinear fiber optics, and all-optical signal processing. From February 2009 to 2011, he was with the Tera-Photonics Group, led by Prof. H. Ito in RIKEN, Sendai, Japan, as a Research Scientist conducting research on terahertz-wave generation, detection, and application using nonlinear optical technologies. Since March 2011, he has been a Professor with the School of Optical and Electronic Information, Wuhan National Laboratory for Optoelectronics, HUST. His current research interests are concerned with optical fiber-based linear and nonlinear effects for communication and sensing applications.

Prof. Tang has been a member of the IEEE Photonics Society since 2001.